Atomic Spectroscopy

Article

Computational And Experimental Studies On Methylene Blue Dye For Sunlight-Driven Photodegradation

Shanty Mathew[a*], Asha A[a], Mohan A[a], Anjana Vinod[a], Tobin Varkey Simson, Anna Kuriakose [a], Elangovan [b], H. Kathyayini[c]
[a]St. Joseph's Research Institute, Lalbagh Road, Bengaluru
[b]Research Centre for Computational and Theoretical Chemistry (RCTC), Tiruchirappalli District,Tamilnadu, India

ABSTRACT: Using modified Hummer's method, nanographene oxide (NGO) was synthesized from graphite flakes. The Mn3O4 nanoparticles were synthesized by precipitation method. The NGO-Mn3O4 nanocomposite synthesis was mediated by bottom-up method. The composite NGO-Mn3O4 was characterized using instrumental techniques including PXRD, SEM, FTIR, UV Reflectance studies, TGA, and DSC. Computational studies were done for methylene blue. The photodegradation studies of methylene blue were carried out using this nanocomposite under sunlight irradiation. While NGO was active in the photodegradation of methylene blue, NGO-Mn3O4 showed better activity than the pure Mn3O4 photocatalyst. Kinetics studies were conducted to determine the reaction's order and rate.

Keywords: Nanographene oxide, nanocomposite of nanographene oxide- Mn3O4, sun light driven photodegradation of methylene blue

INTRODUCTION

Photocatalysis aids in many environmentally friendly applications such as the photodegradation of industrial dyes which are highly toxic to the environment[1]. Dyes have been used immensely in the current technological era in various fields like textile, tarnishing, leather, paint, and food manufacturing and packing industries[2–4]. Dyes when reduced can be converted to aromatic amines which are carcinogenic to humans. It can lead to contact dermatitis, liver and bladder cancers. Therefore, these dyes have to be eradicated before releasing industrial wastewater into the water bodies [5–7]. To facilitate this process, a photodegradation can be carried out using nano-graphene oxide and metal oxide nanocomposites which have similar band gap structures as compared to the HOMO – LUMO energy gaps of these dyes[8]. Methylene blue (MB) is one such cationic dye that is used in the textile industry for dying wool, silks, and cotton. Current research focuses on the degradation of this dye via photocatalysis[9,10] . Photocatalysis has a widespread application in solving major environmental issues such as the degradation of pollutants and toxins released into water bodies, control of global warming, climate change, and useful application of sustainable and clean solar energy into the technological realms [11].

Graphene oxide (GO) and reduced graphene oxide (rGO) are graphene-based compounds with oxygen functionalities in their structure [12–14]. These structures have high porosity, higher surface area, and better dispensability in water and other organic solvents additionally, they have an affinity towards the photo-generated electrons and thus aid in increasing the hole-electron separation lifetime when they are coupled with semiconductors. Therefore, they act as good catalytic support in photocatalysis. They also have a reasonable photocatalytic ability due to their varying bandgap energy and thus better light absorption.

Among the first-row transition elements, oxides of zinc , titanium and manganese are used as oxidants, adsorbents, and degradants[15–18]. Mn_2O_3 and Mn_3O_4 are the oxides of manganese that can be synthesized using MnO_2 by calcination. This research focuses on the synthesis of the composite NGO/Mn_3O_4 semiconductor, characterization, and application in the degradation of an industrial dye, methylene blue. Photodegradation studies are carried out under sunlight irradiation to maximize efficiency and energy consumption. This study is also aimed at understanding the kinetics of this reaction.

EXPERIMENTAL

Nano Graphene oxide (NGO)

Graphite and $NaNO_3$ were mixed with H_2SO_4 and H_3PO_4 and stirred in an ice bath for 10 minutes. $KMnO_4$ was slowly added at 5˚C. The suspension was reacted for 2h in an ice bath and stirred for 60 minutes. It was then stirred in a water bath maintained at 40˚C temperature for 60 minutes. H_2O_2 was added after 5 minutes. Centrifuged and washed with 5% HCl and deionized water. Product was dried at 60˚C. The product is subjected to ultra-sonication in water solvent for about 4hours. GO powder is dispersed in water. Brown dispersion of GO was centrifuged to remove un-exfoliated graphite oxide. Dried overnight at 60˚C and GO was collected.

Trimanganese Tetraoxide (Mn_3O_4)

$MnCl_2$. $4H_2O$ is used as a manganese precursor. NaOH is used as a precipitant. To the prepared Mn solution, the NaOH solution was added dropwise under constant stirring at room temperature which results in the formation of the precipitate. The precipitate was then stirred for 30 mins at room temperature. The solution was then aged under static conditions for around 24 hours. The solution thus obtained was filtered under suction and washed with double distilled water. The product was dried in a hot-air oven pre-set to the temperature of around 100^0C overnight. It was cooled to obtain a brown powder. The product was subjected to calcination at 350^oC temperature

$6\ NaOH + 3\ MnCl_2.\ 4H_2O \rightarrow Mn_3O_4 + 14\ H_2O + 6\ NaCl + H_2$

Nanocomposite

A mixture of Mn_3O_4 and GO in the weight ratio 1:1 was dispersed in the acetone solvent and subjected to ultra-sonication for 3 hours. The dispersed solution is left to evaporate and a pure Mn_3O_4/NGO nanocomposite was obtained.

Characterisation

Powder X- ray patterns of NGO, Mn_3O_4 and NGO/Mn_3O_4 nanocomposite were recorded on a Philips X'pert Pro X-ray diffractometer using Cu–Kα (λ=1.54 Å) using a graphite monochromator to filter the K_β lines. Data were collected at a scan rate of 2° min^{-1} with a 0.02 stepsize for 2θ ranging 5°–70°, to check the formation of nanographene oxide and any new phase formation in the composite. Crystallite size was calculated using Debye–Scherrer equation. The surface morphology of the materials was recorded by scanning electron microscope using Quanta 200 FEI instrument. Infrared spectra of both the samples were recorded using Nicolet IR 200 FTIR spectrophotometer by KBr pellet technique to find the oxygen functionalities present in NGO and the presence of metal-oxygen bond. Thermogravimetric analysis and differential scanning calorimetry analysis were conducted using Perkin Elmer Research Grade; model ST 6000, to study thermal stability by heating over a range of 50–500°C

Computational methods conformational analysis was done with the help of the Vconf program. The Gaussian and Gauss view software produced the optimized structure structural characteristics. The Gaussian software we used to do the NLO characteristics, electronic spectral, HOMO-LUMO and MEP orbital evaluation in various solvents. Multiwfn software was used to figure out TA molecule ELF, ALIE, and LOL. Using Multiwfn and VMD tools, the hydrogen bond interaction was confirmed. Gaussian software was used to figure out the titled molecule physical properties. The molecular docking was done with Autodock-4, and the structure was made by discovery studio Visualized and Ligplot.

Photocatalytic activity studies

In a typical procedure, 10 mg of catalyst was taken in a beaker and stirred with 50 ml of 21 ppm methylene blue solution in the sunlight. The absorbance was measured at every 30-minute interval using Shimadzu – 26001 UV Spectrophotometer at 650nm. In the table, the results are given.

RESULTS AND DISCUSSIONS

Powder X-Ray Diffraction

PXRD patterns of graphite, NGO, Mn_3O_4, and NGO/Mn_3O_4 are given in Figure 1. The characteristic graphite peak at 2θ =27 ° is absent in the PXRD of graphene oxide indicating that graphite is successfully converted to graphene oxide by modified Hummer's method. Moreover, the presence of an XRD peak at 2θ 10.4° value further confirms the formation of graphene oxide. XRD patterns of Mn_3O_4 nanoparticles showed peaks at 18°, 29°, 32°, 36°, 38°, 44°, 50°, 58°, 59°, and 64° which are in good agreement with JCPDS files, which attributes to its tetragonal structure [19]. All the peaks present in NGO-Mn_3O_4 nanocomposites is due to NGO and Mn_3O_4 nanoparticles, no impurity phases are observed indicating the high purity of the nanocomposite. There was no characteristic peak of Mn_3O_4 in the nanocomposite indicating that the Mn_3O_4 particles are well dispersed between the sheets of graphene oxide [20].

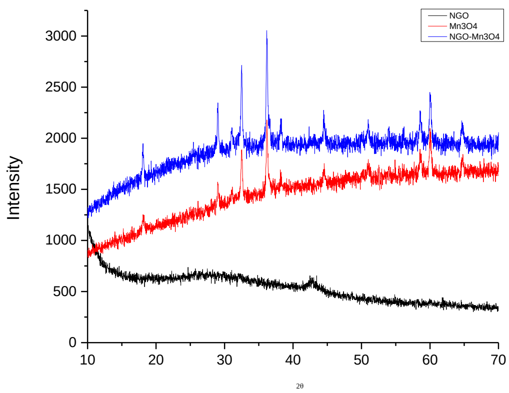

Fig 1. PXRD pattern of NGO, Mn_3O_4 and NGO/Mn_3O_4 composites

Fourier Transform Infrared spectral (FTIR) analysis.

Spectral data gives information on the functional groups attached to the surfaces of the two components NGO and Mn_3O_4, forming the composites (figure 2). Broad peak around 3400cm^{-1} to 3300 cm^{-1} assigned to symmetric stretching vibration of hydroxyl group [21]. C-H stretching vibrational modes appear at 2887 cm^{-1}. Carbonyl or carboxyl peaks appear at 1705 cm^{-1}. C=C stretching shows peak at 1587 cm^{-1}. 1101 and 1068 cm^{-1} peaks correspond to C-O vibrational modes in the Mn-O-C bond. Mn-O stretching modes occurs around 600 to 500 cm^{-1}.

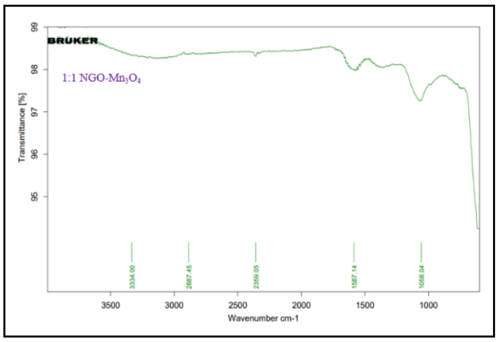

Fig.2 FTIR of NGO/Mn_3O_4

Scanning Electron Micrographs of GO and composites.

Fig 3 (a), (b) show the SEM images of GO whereas figures 3 (c) and (d) shows the SEM images of Mn_3O_4. SEM images of GO appeared to be of sheet like layers whereas SEM images of Mn_3O_4 were granular with different sizes and shapes. It is possible to see the nanoparticles of Mn_3O_4 well disperse on the layers of graphene oxide.

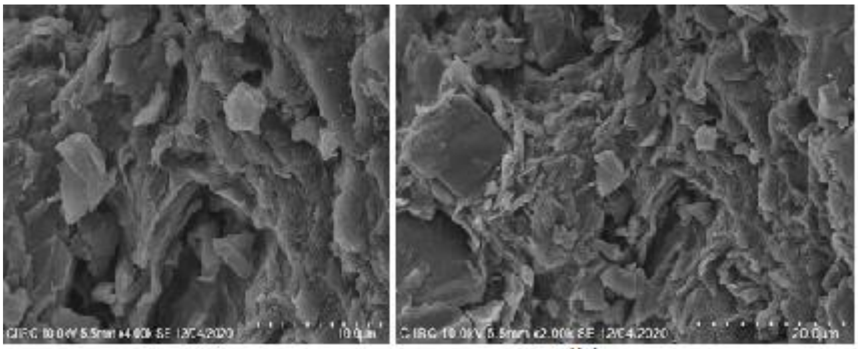

Fig.3(a) Fig.3(b)

Fig 3(a) and 3(b) SEM image of NGO

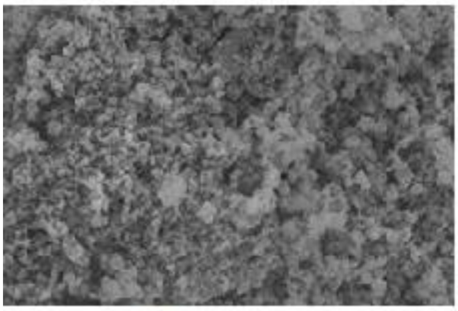

Fig.3(c)

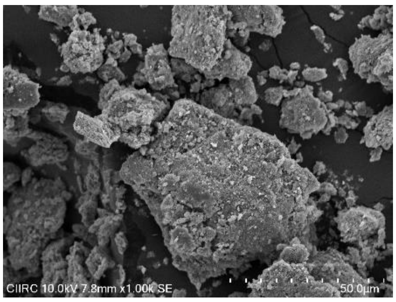

Fig 3(d)

Fig 3(c) and 3(d) SEM images of Mn_3O_4 and NGO- Mn_3O_4 **composites.**

Thermogravimetric Analysis/Differential Scanning caloriemetry (TGA/DSC)

TGA and DSC of $Mn(OH)_2$ are given in figure 4 (a) and (b) respectively. There was a continuous weight loss on heating $Mn(OH)_2$ sample. The various weight loss corresponds to various changes it underwent on heat treatment. Initially $Mn(OH)_2$ lost physisorbed water and the chemisorbed water. Further it was converted to Mn_2O_3 and Mn_3O_4 at different temperatures.

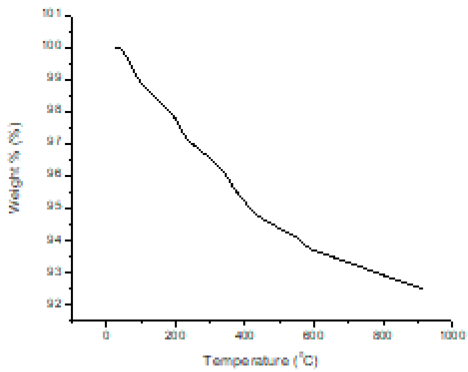

Fig 4a

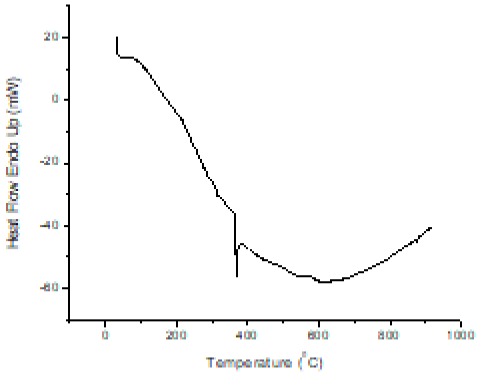

Fig 4b

Ultraviolet – Differential reflectance Spectroscopy (UV-DRS)

The methylene blue has the maximum absorption at 665 nm and therefore has an absorption energy between 1.80 eV to 1.90 eV. The band gap values of NGO, Mn_3O_4 and NGO-Mn_3O_4 are given in table 1. The band gap of NGO is least and that of Mn_3O_4 nanoparticles is highest [22]. The bandgap energy of the composite 1.90 eV is matching with that of methylene blue[23]. Therefore, the band gap energy matching is the reason for the photocatalytic degradation of the dye under sunlight irradiation. The Tauc plot for Mn3O4, NGO and NGO-Mn3O4 particles are given in fig 5 a, b and c respectively.

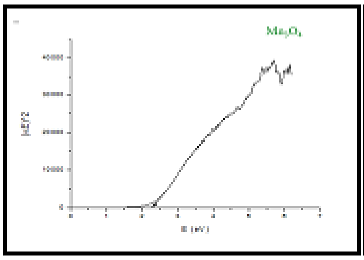

Fig 5a

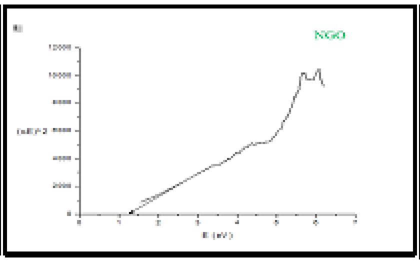

Fig 5b

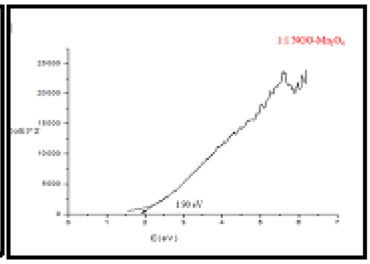

Fig 5 c

Samples	The band gap in eV
NGO	1.25
Mn_3O_4	2.4
NGO-Mn_3O_4 Composite	1.90

Table1. Band gap values of different materials prepared

Photocatalytic activity studies

In our earlier paper, it is reported that NGO is a good photocatalyst for the degradation of Rhodamine 6 B dye . The same trend is observed with the current dye, methylene blue. In this work, it is noticed that the metal oxide Mn_3O_4 is not very catalytically active in the degradation of methylene blue and is more active in making a composite with Mn_3O_4.

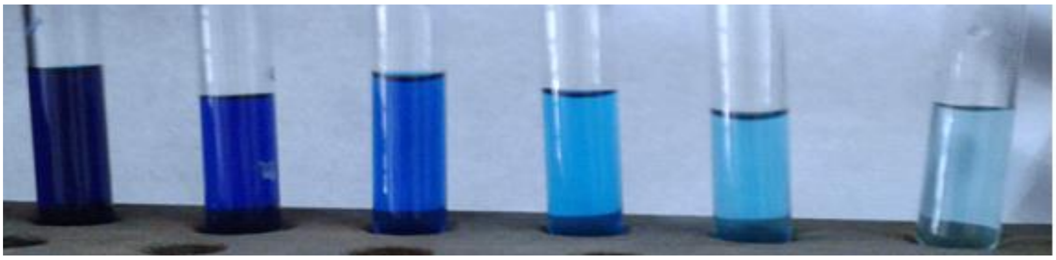

Fig 6 : MB color changes after degradation

Photodegradation of methylene Blue

Degradation was carried under sunlight irradiation between the months of January to April where the average temperature 28 ºC. Constant degradation in the intensity of methylene blue was observed. The solution was kept under dark to equilibrate the sample for an hour before the exposure to sunlight. The results show that NGO is active. The activity of NGO-Mn_3O_4

composite lies between that of their individual activity showing that there is a synergistic behavior between NGO and Mn_3O_4. Photodegradation of nGO, Mn_3O_4 and NGO/Mn_3O_4 follows the order as illustrated below:
NGO > NGO/Mn_3O_4 > Mn_3O_4

Exposure Time (min)	%Degradation		
	NGO	Mn_3O_4	NGO/ Mn_3O_4
0	0	0	0
30	64.7	13.7	33.6
60	71.2	27.5	51.2
90	76.7	47.1	59.7
120	81.5	47.6	63.4
150	85.7	57.6	70.6
180	87.0	66.1	79.6
210	88.4	69.3	85.7
240	89.1	78.8	90.2

Table 2. The % degradation of methylene blue over NGO, Mn_3O_4 and NGO/Mn_3O_4

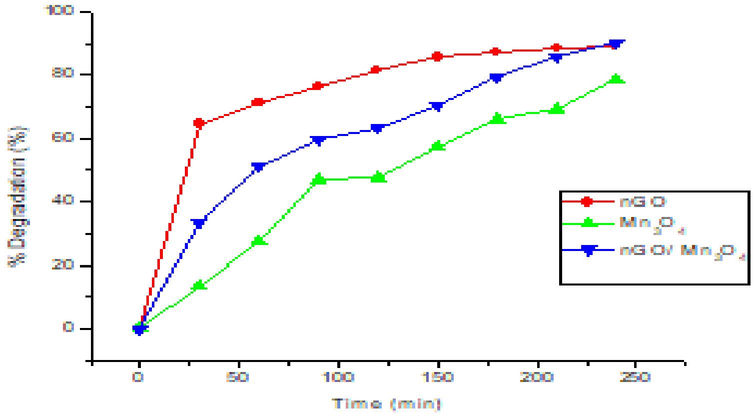

Fig 7. Plot of % degradation vs Time

Kinetic studies
The kinetic studies were carried out for the dye solution at its highest concentration and the results are tabulated and are plotted.

Time (min)	[A] (ppm)	Ln (A/A0)
0	19.35	0.0000
30	12.84	-0.1781
60	9.44	-0.3117
90	7.79	-0.3951
120	7.08	-0.4366
150	5.69	-0.5316
180	3.94	-0.6912
210	2.76	-0.8458
240	1.90	-1.0079

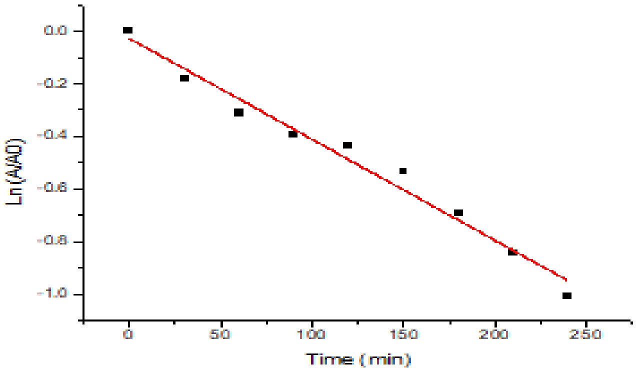

Fig 8 . Plot of ln A/A_0 against time

The plot shows that the reaction follows first order kinetics with rate constant, k value -0.00385 min^{-1}.

Frontier molecular orbital analysis

Frontier molecular orbitals HOMO and LUMO provide electrical, optical, and reactivity information about molecules. Orbital energies predict compound stability and reactivity [24]. The energy gap between HOMO and LUMO orbitals affects molecule stability, charge transfer, chemical activity, softness, and hardness. Smaller energy gaps between HOMO and LUMO allow electron excitation, chemical softness, reactivity, and instability. Bigger energy gaps indicate harder electron excitation, lower chemical reactivity, hardness, and stability. Fig.9 depicts the title compound HOMO-LUMO orbitals [25]. As shown in the Fig.9, the LUMO orbitals cover the two-benzene ring, while the HOMO orbitals change place and cover the benzene ring, sulphur atom and nitrogen atom. This is strong evidence of intramolecular charge transfer. Table.2 lists HOMO and LUMO energy-based global reactivity descriptors [26]. HOMO and LUMO energy gap values for this compound are 1.68 eV. Table.2 list the other parameters and values. The methylene molecule has higher chemical reactivity, lower dynamic stability, more polarizability, and softness due to it 1.68 eV energy gap[27]. HOMO-LUMO charge transfer is easy. The molecule energy gap matches many biomaterials' optical absorption. The compound has high electrophilicity (3.70 eV) and good biological activity.

Table.2 Frontier molecular orbital properties of methylene blue

Property	Values
εHOMO	-6.55
εLUMO	-4.87
Energy gap ΔE	1.68
Ionisation energy (*I*= εHOMO= -HOMO)	6.55
Electron Affinity (*A*= εLUMO= -LUMO)	4.87
Global hardness (Ƞ = (*I*-*A*)/2)	0.84
Global softness (*S* =*1/Ƞ)*	1.19
Chemical Potential (μ = -(I+*A*)/2)	-5.71
Electronegativity (χ = -μ)	5.71
Electrophilicity index (ω = μ2/2Ƞ)	3.70
Nucleophilicity index (*N* = 1/ω)	0.27
Electronaccepting power (ω+ = *A*2/2(*I*-*A*)	1.44
Electrondonating power (ω+ = *I*2/2(*I*-*A*)	1.94

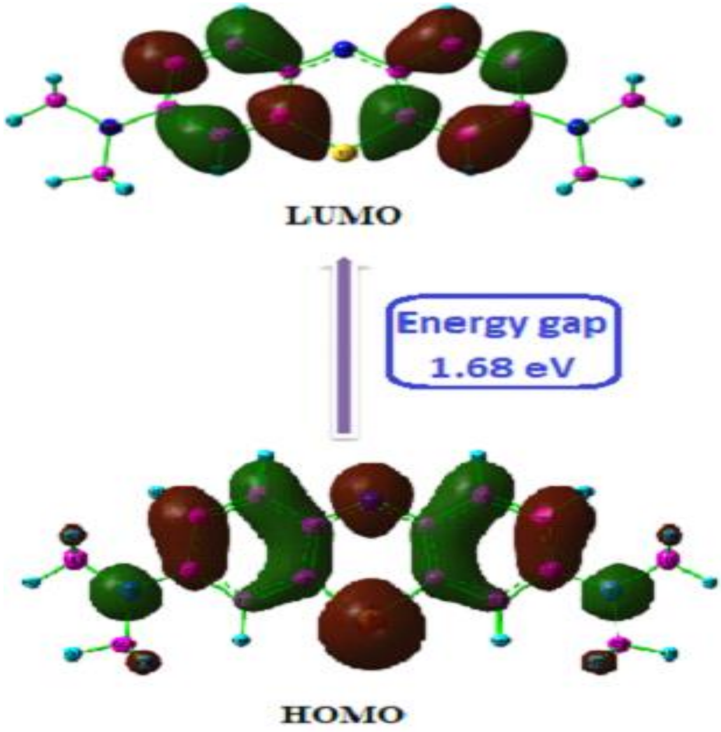

Fig.9 HOMO-LUMO energy diagram of methylene blue

Molecular electrostatic potential

The MEP analysis have been used in this section to investigate the charge distribution on the molecular surface as well as the atoms. The MEP maps provide some insight into the chemical reactivities of the compounds, by identifying electrophilic and nucleophilic attack regions in the molecule in accordance with charge distributions [28]. The region that is the deepest red reveals the charged positions that are the most negatively charged, whereas the region that is the deepest blue reveals the charged positions that are the most positively charged [29]. The yellow regions indicate slightly negatively charged positions, whereas the cyan regions indicate slightly positively charged positions. Green surfaces indicate areas with zero electrostatic potential. As can be seen in Fig.10, the regions of the map with a negative potential have been distributed across nitrogen atom for this compound [30]. As a result, these regions are vulnerable to electrophilic attacks. The regions with a positive potential have been dispersed throughout the methyl group attached nitrogen atom and sulphur atom. These regions are good spots for nucleophilic attacks to take place [31]. The colour of these regions, on the other hand, is not a dark blue; as a result, we cannot say that these regions are strong nucleophilic regions.

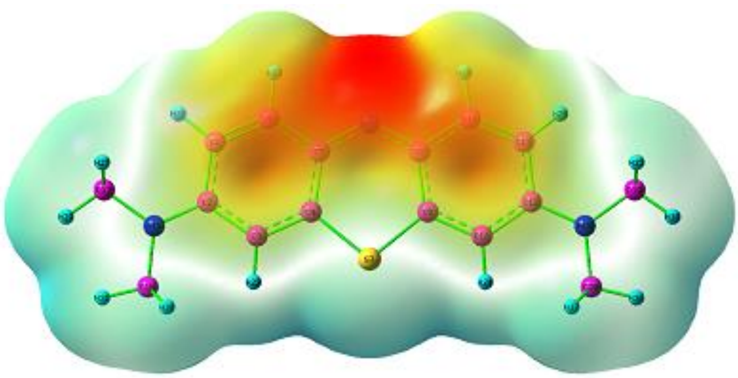

Fig.10 Molecular electrostatic potential surface amp of the titled compound

CONCLUSION

NGO is a good photocatalyst for the removal of methylene blue. Mn_3O_4 degrade methylene blue but not to the extent of NGO. However, when a nanocomposite of NGO/ Mn_3O_4 is prepared and studied for the photodegradation of methylene blue the ability of the composite was better than either of the two. The photocatalytic activity of Mn_3O_4 which was very poor become equal to NGO activity on exposure to sunlight for irradiation of 240 mins. Preparation of NGO involves tedious method, however, Mn_3O_4 can be synthesized very easily by precipitation and calcination. So instead of using NGO alone a nanocomposite of NGO/ Mn_3O_4 will give the same result as NGO alone. This result shows that the band gap required for the degradation of methylene blue is suitable with NGO and not that of Mn_3O_4 however when the composite is prepared the band gap of the composited is tuned to match for the degradation. So here there is a synergetic effect of the two. The order of the reaction is found to be first order. Hence the nanocomposite /nGO Mn_3O_4 is a promising catalyst for the degradation of dyes.

DECLARATION OF COMPETING INTEREST

The authors declare that they have no competing interests

REFERENCES

1. J.F. Leal, S.M.A. Cruz, B.T.A. Almeida, V.I. Esteves, P.A.A.P. Marques, E.B.H. Santos, TiO_2-rGO nanocomposite as an efficient catalyst to photodegrade formalin in aquaculture's waters, under solar light, Environ. Sci. Water Res. Technol. 6 (2020) 1018–1027. https://doi.org/10.1039/C9EW00950G.
2. [2] M. Ubaidullah, A.M. Al-Enizi, A. Nafady, S.F. Shaikh, K.Y. Kumar, M.K. Prashanth, L. Parashuram, B.-H. Jeon, M.S. Raghu, B. Pandit, Photocatalytic CO_2 reduction and pesticide degradation over g-C_3N_4/Ce_2S_3 heterojunction, J. Environ. Chem. Eng. 11 (2023) 109675. https://doi.org/10.1016/J.JECE.2023.109675.
3. [3] Y. Li, H. Huang, R. Cui, D. Wang, Z. Yin, D. Wang, L. Zheng, J. Zhang, Y. Zhao, H. Yuan, J. Dong, X. Guo, B. Sun, Electrochemical sensor based on graphdiyne is effectively used to determine Cd^{2+} and Pb^{+2} in water, Sensors Actuators, B Chem. 332 (2021) 129519. https://doi.org/10.1016/j.snb.2021.129519.
4. [4] K. Mallikarjuna, O. Nasif, S.A. Alharbi, S. V. Chinni, L.V. Reddy, M.R.V. Reddy, S. Sreeramanan, Phytogenic synthesis of Pd-Ag/rGO nanostructures using stevia leaf extract for photocatalytic H2 production and antibacterial studies, Biomolecules. 11 (2021) 1–15. https://doi.org/10.3390/biom11020190.
5. [5] Y. Yang, L. Cao, S. Wu, L. Qin, S. Kang, X. Li, A patterned aluminum/reduced graphene oxide/silver sheet for detection and degradation of malachite green in water, Sep. Purif. Technol. 272 (2021) 118892. https://doi.org/10.1016/j.seppur.2021.118892.
6. [6] S. Akshatha, S. Sreenivasa, L. Parashuram, V. Udaya kumar, F.A. Alharthi, T.M. Chakrapani Rao, S. kumar, Microwave assisted green synthesis of p-type Co_3O_4@Mesoporous carbon spheres for simultaneous degradation of dyes and photocatalytic hydrogen evolution reaction, Mater. Sci. Semicond. Process. 121 (2021) 105432. https://doi.org/10.1016/j.mssp.2020.105432.
7. [7] N. Belachew, M.H. Kahsay, A. Tadesse, K. Basavaiah, Green synthesis of reduced graphene oxide grafted Ag/ZnO for photocatalytic abatement of methylene blue and antibacterial activities, J. Environ. Chem. Eng. 8 (2020) 104106. https://doi.org/10.1016/j.jece.2020.104106.
8. [8] M. Xu, Y. Wang, E. Ha, H. Zhang, C. Li, Reduced graphene oxide/$Bi_4O_5Br_2$ nanocomposite with synergetic effects on improving adsorption and photocatalytic activity for the degradation of antibiotics, Chemosphere. 265 (2021) 129013. https://doi.org/10.1016/j.chemosphere.2020.129013.
9. [9] K. Chaudhary, M. Aadil, S. Zulfiqar, S. Ullah, S. Haider, P.O. Agboola, M.F. Warsi, I. Shakir, Graphene oxide and reduced graphene oxide supported ZnO nanochips for removal of basic dyes from the industrial effluents, Fullerenes Nanotub. Carbon Nanostructures. 29 (2021) 915–928. https://doi.org/10.1080/1536383X.2021.1917553.
10. [10] K. Yogesh Kumar, L. Parashuram, M.K. Prashanth, C.B. Pradeep Kumar, F.A. Alharti, P. Krishnaiah, B.H. Jeon, M. Govindasamy, M.S. Raghu, N-doped reduced graphene oxide anchored with δTa_2O_5 for energy and environmental remediation: Efficient light-driven hydrogen evolution and simultaneous degradation of textile dyes, Adv. Powder Technol. 32 (2021) 2202–2212. https://doi.org/10.1016/j.apt.2021.04.031.
11. [11] S. Hamzad, K.Y. Kumar, M.K. Prashanth, D. Radhika, L. Parashuram, F.A. Alharti, B.H. Jeon, M.S. Raghu, Boron doped RGO from discharged dry cells decorated Niobium pentoxide for enhanced visible light-induced hydrogen evolution and water decontamination, Surfaces and Interfaces. 36 (2023) 102544. https://doi.org/10.1016/j.surfin.2022.102544.
12. [12] P. Yadav, P.K. Surolia, D. Vaya, Synthesis and application of copper ferrite-graphene oxide nanocomposite photocatalyst for the degradation of malachite green, Mater. Today Proc. 43 (2021) 2949–2953. https://doi.org/10.1016/j.matpr.2021.01.301.
13. [13] T. de Figueiredo Neves, N. Barticiotto Dalarme, P.M.M. da Silva, R. Landers, C. Siqueira Franco Picone, P. Prediger, Novel magnetic chitosan/quaternary ammonium salt graphene oxide composite applied to dye removal, J. Environ. Chem. Eng. 8 (2020) 103820. https://doi.org/10.1016/j.jece.2020.103820.
14. [14] M. Gaidi, K. Daoudi, S. Columbus, A. Hajjaji, M.A. El Khakani, B. Bessais, Enhanced photocatalytic activities of silicon nanowires/graphene oxide nanocomposite: Effect of etching parameters, J. Environ. Sci. (China). 101 (2021) 123–134. https://doi.org/10.1016/j.jes.2020.08.010.
15. [15] S. Bibi, A. Ahmad, M.A.R. Anjum, A. Haleem, M. Siddiq, S.S. Shah, A. Al Kahtani, Photocatalytic degradation of malachite green and methylene blue over reduced graphene oxide (rGO) based metal oxides (rGO-Fe_3O_4/TiO_2) nanocomposite under UV-visible light irradiation, J. Environ. Chem. Eng. 9 (2021). https://doi.org/10.1016/j.jece.2021.105580.
16. [16] T.A. Kurniawan, Z. Mengting, D. Fu, S.K. Yeap, M.H.D. Othman, R. Avtar, T. Ouyang, Functionalizing TiO_2 with graphene oxide for enhancing photocatalytic degradation of methylene blue (MB) in contaminated wastewater, J. Environ. Manage. 270 (2020) 110871. https://doi.org/10.1016/j.jenvman.2020.110871.
17. [17] T. Naseem, Zain-ul-Abdin, M. Waseem, M. Hafeez, S.U. Din, S. Haq, Mahfoz-ur-Rehman, Reduced Graphene Oxide/Zinc Oxide Nanocomposite: From Synthesis to its Application for Wastewater Purification and Antibacterial Activity, J. Inorg. Organomet. Polym. Mater. 30 (2020) 3907–3919. https://doi.org/10.1007/s10904-020-01529-2.

18. [18] R. Suresh, R. V. Mangalaraja, H.D. Mansilla, P. Santander, J. Yáñez, Reduced Graphene Oxide-Based Photocatalysis, (2020) 145–166. https://doi.org/10.1007/978-3-030-15608-4_6.
19. [19] K. Zhang, H. Zeng, J. Feng, Z. Liu, Z. Chu, W. Jin, Screen-printing of core-shell Mn_3O_4@C nanocubes based sensing microchip performing ultrasensitive recognition of allura red, Food Chem. Toxicol. 162 (2022) 112908. https://doi.org/10.1016/j.fct.2022.112908.
20. [20] M.F. Elshahawy, G.A. Mahmoud, A.I. Raafat, A.E.H. Ali, E. said A. Soliman, Fabrication of TiO_2 Reduced Graphene Oxide Based Nanocomposites for Effective of Photocatalytic Decolorization of Dye Effluent, J. Inorg. Organomet. Polym. Mater. 30 (2020) 2720–2735. https://doi.org/10.1007/s10904-020-01463-3.
21. [21] N. Balis, A.A. Zaky, C. Athanasekou, A.M. Silva, E. Sakellis, M. Vasilopoulou, T. Stergiopoulos, A.G. Kontos, P. Falaras, Investigating the role of reduced graphene oxide as a universal additive in planar perovskite solar cells, J. Photochem. Photobiol. A Chem. 386 (2020). https://doi.org/10.1016/j.jphotochem.2019.112141.
22. [22] Krishnamoorthy, K., Mohan, R. and Kim, S.J., 2011. Graphene oxide as a photocatalytic material. Applied Physics Letters, 98(24), p.244101.
23. [23] Wang, J., Zhao, H., Song, J., Zhu, T. and Xu, W., 2019. Structure-Activity Relationship of Manganese Oxide Catalysts for the Catalytic Oxidation of (chloro)-VOCs. Catalysts, 9(9), p.726.
24. [24] N. Elangovan, T.S. Ganesan, B. Rajeswari, A. Kanagavalli, S. Kokilavani, S. Sowrirajan, S. Chandrasekar, R. Thomas, Solid-state Synthesis, electronic Structure Studies, Solvent Interaction through Hydrogen Bonding, and Molecular Docking Studies of 2,2'-((1,2-Phenylenebis(Azaneylylidene))Bis (Methaneylylidene))Diphenol from o-Phenylenediamine and Salicylaldehyde, Polycycl. Aromat. Compd. (2023). https://doi.org/10.1080/10406638.2023.2198723.
25. [25] N. Elangovan, S. Yousef, S. Sowrirajan, B. Rajeswari, A. Nawaz, Photoluminescence property and solvation studies on sulfonamide ; Synthesis , structural , topological analysis , antimicrobial activity and molecular docking studies, Inorg. Chem. Commun. 155 (2023) 111019. https://doi.org/10.1016/j.inoche.2023.111019.
26. [26] P. Parthipan, L. Cheng, A. Rajasekar, M. Govarthanan, A. Subramania, Biologically reduced graphene oxide as a green and easily available photocatalyst for degradation of organic dyes, Environ. Res. 196 (2021). https://doi.org/10.1016/j.envres.2021.110983.
27. [27] N. Elangovan, S. Sowrirajan, A.Y.A. Alzahrani, D.S. Rajendran Nair, R. Thomas, Fluorescent Azomethine by the Condensation of Sulfadiazine and 4-Chlorobenzaldehyde in Solution: Synthesis, Characterization, Solvent Interactions, Electronic Structure, and Biological Activity Prediction, Polycycl. Aromat. Compd. 0 (2023) 1–22. https://doi.org/10.1080/10406638.2023.2216833.
28. [28] G. Thilagavathi, R. Jayachitra, A. Kanagavalli, N. Elangovan, A. Sirajunnisa, S. Sowrirajan, R. Thomas, Journal of the Indian Chemical Society Synthesis , computational , molecular docking studies and photophysical amino) benzenesulfonamide, J. Indian Chem. Soc. 100 (2023) 100835. https://doi.org/10.1016/j.jics.2022.100835.
29. [29] T. Sanakarganesan, N. Elangovan, S. Chandrasekar, E. Ganesan, V. Balachandran, Inorganica Chimica Acta Synthesis , Hirshfeld surface analysis , computational , wave function properties , anticancer and cytotoxicity activity of di [(p-chlorobenzyl), Inorganica Chim. Acta. 547 (2023) 121361. https://doi.org/10.1016/j.ica.2022.121361.
30. [30] İ. Tanişik, Ö. Uğuz, D. Akyüz, R.M. Zunain Ayaz, C. Sarioğlu, F. Karaca, A.R. Özkaya, A. Koca, Solar-hydrogen production with reduced graphene oxide supported CdxZn1-xS photocatalysts, Int. J. Hydrogen Energy. 45 (2020) 34845–34856. https://doi.org/10.1016/j.ijhydene.2020.04.035.
31. [31] K.J. Rajimon, N. Elangovan, A. Amir, R. Thomas, Schiff bases from chlorine substituted anilines and salicylaldehyde : Synthesis , characterization , fluorescence , thermal features , biological studies and electronic structure investigations, J. Mol. Liq. 370 (2023) 121055. https://doi.org/10.1016/j.molliq.2022.121055